Unraveling the discontinuous plastic flow of a Co-Cr-Fe-Ni-Mo multiprincipal-element alloy at deep cryogenic temperatures

Jongun Moon,[1] Elena Tabachnikova [ORCID],[2] Sergii Shumilin,[2] Tetiana Hryhorova [ORCID],[2] Yuri Estrin [ORCID],[3,4] Jamieson Brechtl [ORCID],[5] Peter K. Liaw [ORCID],[6] Wenqing Wang,[7] Karin A. Dahmen,[7] and Hyoung Seop Kim [ORCID][1,8,9,*]

[1]*Department of Materials Science and Engineering, Pohang University of Science and Technology (POSTECH), Pohang 37673, Korea*
[2]*B. Verkin Institute for Low Temperature Physics and Engineering of National Academy of Sciences of Ukraine, Kharkov, 61103, Ukraine*
[3]*Department of Materials Science and Engineering, Monash University, Clayton VIC 3800, Australia*
[4]*Department of Mechanical Engineering, The University of Western Australia, Crawley, WA 6009, Australia*
[5]*The Bredesen Center for Interdisciplinary Research and Graduate Education, The University of Tennessee, Knoxville, Tennessee 37996, USA*
[6]*Department of Materials Science and Engineering, The University of Tennessee, Knoxville, Tennessee 37996, USA*
[7]*Department of Physics, University of Illinois at Urbana-Champaign, 1110 West Green Street, Urbana, Illinois 61801, USA*
[8]*Graduate Institute of Ferrous Technology, Pohang University of Science and Technology (POSTECH), Pohang 37673, Korea*
[9]*Center for High Entropy Alloys, Pohang University of Science and Technology (POSTECH), Pohang 37673, Korea*

We report an analysis of the discontinuous plastic flow of a multiprincipal-element alloy, $Co_{17.5}Cr_{12.5}Fe_{55}Ni_{10}Mo_5$ (atomic percent, at. %), in the temperature range of 0.5–4.2 K showing serrated deformation curves. Using the analytical techniques, we studied the statistics of the stress drops associated with the unstable plastic flow. The analysis showed that the complexity and heterogeneity of a discontinuous plastic flow were reduced when the temperature was lowered. This behavior was associated with the effects of dynamic recovery and adiabatic heating on the dislocation-density evolution.

I. INTRODUCTION

Possible applications at cryogenic temperatures, down to near-absolute zero, include liquefied natural gas (LNG) storage tanks ($\sim$103 K) [1], cryogenic cargo pumps and valves ($\sim$112 K) [2], and outer-space applications ($\sim$2–3 K) [3]. At cryogenic temperatures, a discontinuous plastic flow (DPF) is a prominent feature of face-centered-cubic (fcc) metals and alloys [4–8]. The low-temperature DPF is associated with the formation of dislocation pileups at internal barriers to their motion (e.g., Lomer-Cottrell locks, grain boundaries, shear bands, etc.), which create stress concentrations [6,9–13]. Below a certain critical temperature, the dislocations cannot escape a pileup through cross slip because of a deficit in the thermal energy for the generation and motion of screw dislocations. This trend leads to a transition of the predominant dislocation character from the screw to edge type [9,14,15]. As a result, stress drops occur as a response to the plastic-strain bursts due to the avalanchelike barrier crossing by dislocations, referred to as avalanche slips [9,11,14–16]. Repeated stress drops give the stress-strain curves their characteristic serrated appearance.

Recently, an exploration of the low-temperature DPF was extended to multiprincipal-element alloys (MPEAs), also known as high-entropy or medium-entropy alloys (HEAs or MEAs) [11,13,17–23]. To date, fcc-based CoCrFeMnNi [17,18], CoCrFeNi [19], $Al_{0.1}CoCrFeNi$ [20], $Ag_{0.5}CoCrCuFeNi$ [11], $Al_{0.5}CoCrCuFeNi$ [13,21], and $CoCrFeMnNiV_x$ ($x = 0$, 0.25, 0.50, and 0.75, mole frac-

tion) [22] MPEAs have been studied to understand their low-temperature DPF. Possible links among the outstanding mechanical properties at cryogenic temperatures, low-temperature DPF, and additional mechanisms involved in the deformation process, such as stacking-fault formation, deformation-induced twinning, and phase transformation, have been examined for the aforementioned HEAs [23].

In our previous work [24], it was shown that a $Co_{17.5}Cr_{12.5}Fe_{55}Ni_{10}Mo_5$ MPEA (atomic percent, at. %, henceforth referred to as Mo5) exhibits an excellent combination of strength and ductility at cryogenic temperatures down to 0.5 K owing to precipitation hardening and deformation-induced martensitic transformation (DIMT). In the temperature range from 0.5 to 4.2 K, the plastic flow of the Mo5 alloy is discontinuous and is accompanied with an anomalous temperature dependence of DIMT [24]. During deformation of the Mo5 alloy at 4.2 K, the predominance of edge-type dislocations inhibits DIMT and dynamic recovery [24]. However, below 4.2 K, the heat generation during DPF, which can be considered as nearly adiabatic, increases the temperature inside the localized shear bands, which results in the activation of screw dislocations [24]. Due to this effect, DIMT and dynamic recovery do take place during deformation of the Mo5 alloy below the liquid helium temperature [24]. This trend leads to a reduction in the local dislocation density within the slip bands. Since the complexity of the low-temperature deformation behavior of the Mo5 alloy is compounded by the occurrence of thermomechanical coupling and the ensuing thermal instability, understanding DPF of the Mo5 alloy is a challenging task. (We note that in the temperature range of interest, quantum effects may play a role in the dislocation dynamics [25], which would further complicate the

*hskim@postech.ac.kr
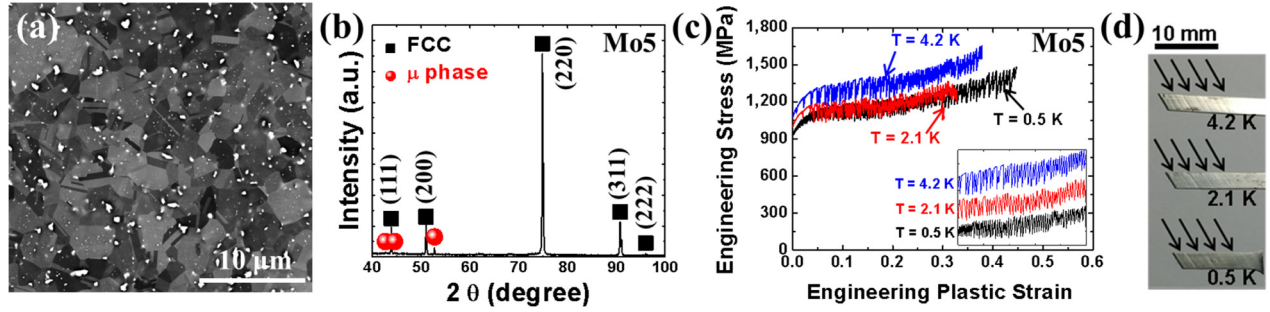
FIG. 1. Initial microstructure of the Mo5 alloy: (a) SEM-BSE image and (b) XRD of the annealed Mo5 alloy. The white particles in (a) were identified as μ precipitates. (c) Engineering stress-strain curves for the Mo5 alloy showing DPF at 0.5, 2.1, and 4.2 K. The inset in (c) reveals the enlarged and vertically shifted stress-strain curves exhibiting serrations at all three temperatures. (d) Photographs of the deformed tensile specimens at different temperatures. The black arrows in (d) point to localized shear bands.

analysis. However, the contribution of quantum tunneling to the activation energy for kink formation in the Peierls relief was shown to be negligible—apart from the cases when the applied stress is close to the Peierls stress [26].) In the present study, we invoked advanced theoretical techniques to unravel this complexity observed experimentally at low temperatures of 0.5, 2.1, and 4.2 K. To that end, we applied an analysis of the stress-drop statistics, as well as the refined composite multiscale entropy (RCMSE) method, and the multifractal detrended fluctuation analysis (MFDFA) algorithm.

II. EXPERIMENTAL METHODS AND RESULTS

The cold-rolled and annealed Mo5 plate was prepared through the same fabrication route as in Ref. [24]. Dog-bone shaped tensile specimens with a gauge length of 15 mm and a width of 3 mm were fabricated from the annealed plate for tensile testing. The surfaces of the tensile specimens were mechanically polished up to 1200 SiC grit paper. Tensile tests at a strain rate of 10^{-4} s^{-1} were conducted at 0.5, 2.1, and 4.2 K. To ensure reproducibility of the results, the experiments were carried out in triplicate. The temperature was measured with a semiconductor thermometer, which was placed close to the tensile sample. The temperature of 77 K was obtained, using liquid nitrogen, with further cooling down to 4.2 K achieved by placing a sample in liquid ^{4}He. The temperatures of 2.1 and 0.5 K were obtained by lowering the pressure above boiling liquids, ^{4}He and ^{3}He, respectively, through additional pumping. The method for obtaining these extremely low temperatures is described in detail in Ref. [27].

Scanning electron microscopy (SEM) with backscattered electron (BSE) analysis was performed, using a field electron and ion Helios 650 device. In addition, x-ray-diffraction (XRD) measurements were carried out, employing a Rigaku D/MAX-2500 device. The SEM-BSE and XRD samples were polished up to 1200 SiC grit paper, and then electropolished in an etchant solution of mixed 92% CH$_3$COOH and 8% HClO$_4$ (volume percent) to remove scratches and a strained layer produced by mechanical polishing. The XRD scans with the incident beam of Cu Kα radiation (wavelength = 1.5418 Å) were conducted in the 2θ range from 40° to 100° with a step size of 0.02° and a scan speed of 2°/min.

The annealed Mo5 alloy contained μ precipitates dispersed in an fcc matrix, as shown in Figs. 1(a) and 1(b). The average

grain size of the fcc grain was 3.82 ± 1.82 μm, while the μ precipitates had the average size of 354.32 ± 125.06 nm and the areal fraction of $3.21 \pm 0.26\%$ [Fig. 1(a)]. The high intensity of the (220) fcc peak in Fig. 1(b) is associated with the retained texture components of the cold-rolled fcc material, such as $\{110\}\langle100\rangle$ Goss and $\{110\}\langle112\rangle$ brass components [28]. It should be noted that the present Mo5 alloy was prepared by severe cold rolling with a thickness reduction from 7 to 0.6 mm [24]. Figure 1(c) shows the tensile curves of the Mo5 alloy at different temperatures: 0.5, 2.1, and 4.2 K. A discontinuous plastic flow of the Mo5 alloy was observed for the two temperatures below 4.2 K. The highest yield strength (1075 MPa) and ultimate tensile strength (1651 MPa) of the alloy were found at 4.2 K. As a function of temperature, the yield strength showed an anomalous trend: it dropped with a decrease in temperature [24]. A prominent feature of the deformation at all three temperatures was the occurrence of localized shear bands, about 50 μm in width, on the surface of the deformed tensile samples [Fig. 1(d)].

III. STRESS-DROP STATISTICS

The stress-drop statistics were analyzed by considering the distribution of the slip-avalanche size and the periodicity of large avalanches. From the observation data, we extracted the size and duration of avalanches. The engineering stress was differentiated with respect to time to obtain the stress rate sequence. An avalanche begins when the stress rate falls below zero. When the stress rate rises above zero, the avalanche is considered to end. The slip avalanche size, S, is defined as the difference in the stress between these two points. The corresponding time difference, T, is referred to as the avalanche duration. The complementary cumulative size distribution (CCDF), denoted $C(S)$ [Fig. 2(a)], gives the probability that an avalanche has a size larger than S. The flat middle section of the $C(S)$ curve, followed by a sharp drop at the high end of $C(S)$, indicates that the material deforms in many large slips with the attendant stress drops larger than 100 MPa.

In many materials with the so called "stick-slip" behavior, this type of steplike CCDF is observed and in those cases, the large events often recur almost periodically (with a few small slips in between). So, we checked whether stress drops with a size above 100 MPa occurred approximately periodically. To
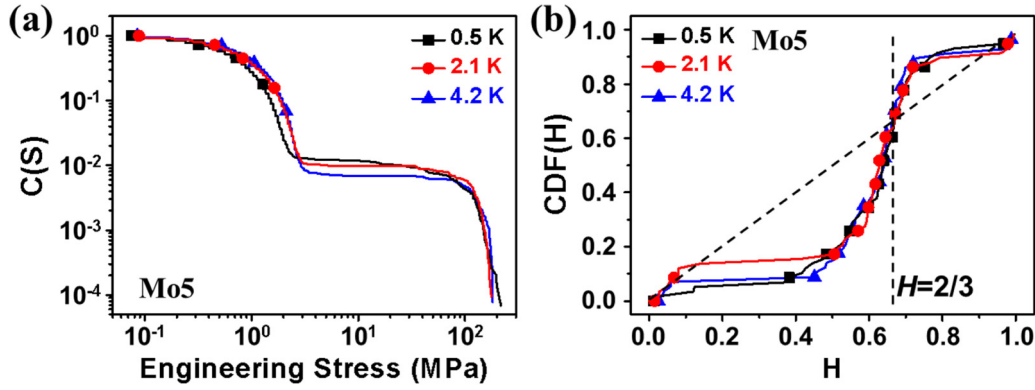
FIG. 2. (a) CCDF, $C(S)$, of avalanches (engineering stress) observed in the Mo5 alloy during tensile deformation at 0.5, 2.1, and 4.2 K. (b) Cumulative distribution function, $CDF(H)$, for the large avalanches, with sizes above 100 MPa, with respect to the H values obtained from the Bi test. The black vertical line corresponds to $H = 2/3$, and the black oblique line indicates a perfect Poisson process.

that end, we conducted a Bi test [29] for the large avalanches considered separately. For each large avalanche, the temporally prior and temporally subsequent interevent times were calculated. The interevent times for a given avalanche are defined as the difference between its starting time and those of two avalanches adjacent to it [30]. The smaller of the two interevent times is denoted as δt_i, and the quantity, $\delta \tau_i$, is the next interevent time in the same temporal direction during the Bi test, as presented below [30]:

$$\delta t_i = \min (t_i - t_{i-1}, \; t_{i+1} - t_i), \tag{1}$$

$$\delta \tau_i = t_{i-1} - t_{i-2} \quad \text{if} \;\; \delta t_i = t_i - t_{i-1}, \tag{2}$$

$$\delta \tau_i = t_{i+2} - t_{i+1} \quad \text{if} \;\; \delta t_i = t_{i+1} - t_i, \tag{3}$$

where t_i is the starting time of the ith avalanche. The cumulative distribution of the quantity, H, represents the interevent time correlations, and its shape is an indication of the degree of periodicity. For each large avalanche with an index, i, H is defined as [30]

$$H_i = \delta t_i / \left(\delta t_i + \frac{\delta \tau_i}{2} \right), \tag{4}$$

where H_i has a value between 0 and 1. If the dataset is consistent with a randomly occurring Poisson process, δt_i and $\delta \tau_i$ will be statistically independent. These quantities are distributed according to the probability density, P, given below [31]:

$$P(\delta t) = 2\lambda_i \exp(-2\lambda_i \delta t_i), \tag{5}$$

$$P(\delta \tau) = \lambda_i \exp(-\lambda_i \delta \tau_i), \tag{6}$$

where λ_i is the local Poissonian rate at time, t_i.

The CDF of the set of H_i fluctuates around a straight line from (0,0) to (1,1) for a Poisson process [29]. If the large avalanches exhibited ideal periodicity, the interevent times were the same, i.e., $H_i = 2/3$ would hold for all i. A steep increase of the cumulative distribution of H near $H = 2/3$ is a clear indication that the avalanches occur *almost* periodically. In Fig. 2(b), we observe such a rapid rise near $H = 2/3$ for all serration data sets recorded for Mo5, and this trend can be

interpreted as a near periodicity of large avalanches in the alloy. A simple analytical model [32–34] for the statistics of serrations in stress-strain curves suggests that almost-periodically recurring large serrations are consistent with a strong weakening mechanism during the slips. The idea is that as the material is slowly deformed, weak spots in the material slip collectively in "slip avalanches". If the local threshold stress for slipping becomes significantly lower during a slip event and reheals after the slip avalanche (somewhat similar to what happens in static versus dynamic friction), then the model predicts the emergence of large, periodically recurring slips. Such behavior is sometimes termed stick-slip and has been seen in many other systems [32–38]. Both the slip statistics shown in $C(S)$ and the Bi test thus suggest that this type of mechanism plays a role in this case, because the data clearly present this type of stick-slip behavior. To better understand the DPF at each individual test temperature, further analytical techniques, *viz.* the RCMSE analysis and the MFDFA, were employed.

IV. RCMSE ANALYSIS

The RCMSE technique has been used to analyze various phenomena, including the chaos [39], physiological data [40,41], and DPF in alloys [23,42–44]. The RCMSE method is suited to examine the complexity of the time-series data, where complexity is associated with a "meaningful structural richness" of a given dataset [45]. More specifically, larger measures of complexity are indicative of more irregular dynamical behavior [46]. Limitations to the RCMSE method include a risk of calculating undefined entropy values, although this risk is low, as compared to other algorithms, such as the multiscale entropy (MSE) method [47]. However, it should be stated that the computational cost of the RCMSE technique is greater than that of the MSE method [48].

In relation to DPF, greater complexity values have been attributed to an increase in the number of interactions that occur during dislocation locking [42]. For example, Sarkar *et al.* observed that the complexity of discontinuous yielding exhibited by a low-carbon steel was significantly larger than that of an Al-Mg alloy [43]. This result was associated with a greater variety of interactions that were occurring in the
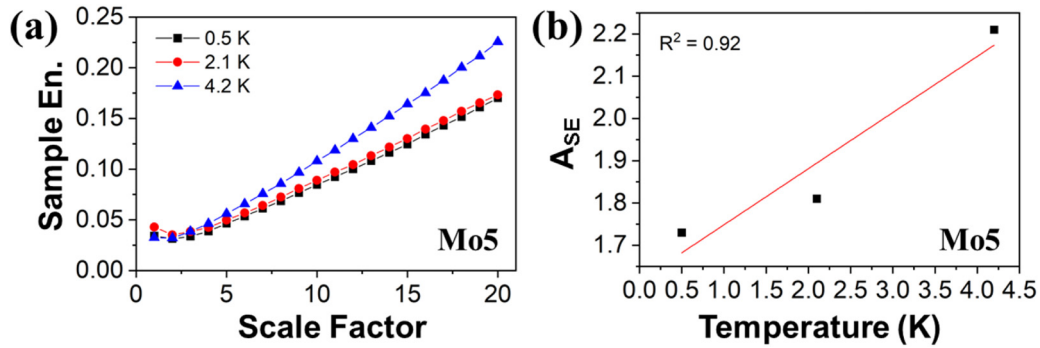
FIG. 3. Results of the RCMSE analysis featuring the (a) sample entropy and (b) the area under the sample entropy curves (A_{SE}) for samples tested at 0.5, 2.1, and 4.2 K.

carbon steel during tension, where interstitial carbon interacts with both screw and edge dislocations. By contrast, substitutional atoms in the Al-Mg alloy can only interact with edge dislocations.

In the present work, the RCMSE method was used to analyze the DPF of the Mo5 alloy in the temperature range of 0.5 to 4.2 K illustrated by the curves in Fig. 1. The detailed procedures of the RCMSE technique are provided in the Supplemental Material [49] and Refs. [46,47]. It is important to note that if the values of the sample entropy for the majority of scale factors are higher for one set of DPF data over another, the former is considered more complex than the latter [46]. Figure 3 presents the results of the RCMSE analysis for the samples tested at 0.5, 2.1, and 4.2 K. As seen from Fig. 3(a), the sample entropy generally increased with respect to the scale factor, indicating that the DPF exhibited complex behavior across multiple scales [42]. Furthermore, the sample entropy curves lay higher for higher test temperatures, which show that the complexity and irregularity of the DPF increased with temperature. To corroborate this feature, the area enclosed under the RCMSE curve (denoted by A_{SE}) was calculated for each temperature condition [42]. The results are displayed in Fig. 3(b), which confirms that the complexity of the DPF did, indeed, increase with increasing temperature. Furthermore, the relatively large R^2 value of 0.92 indicates that there was a high degree of positive correlation between the complexity of the DPF and the temperature. This result signifies that in the temperature range considered, the discontinuous yielding reflected in serrated deformation curves becomes more complex with the rising deformation temperature.

V. MFDFA

A multifractal structure is defined by a multifractal spectrum of power-law exponents that arise from spatial and temporal variations [50]. Such a variation in the scaling behavior can be observed, for example, when a given time series consists of many interwoven fractal subsets [51]. Techniques have been developed to measure the multifractal spectra of a given dataset. Such methods have been used to model and analyze the DPF in different material systems, including Al-Mg alloys [52–58], bulk-metallic glasses [59,60], and HEAs [23,61]. For example, Lebyodkin *et al.* reported that the phase composition and the presence of second-phase particles of

an Al-Mg alloy affected the multifractal characteristics of the DPF [62]. Bharathi *et al.* [53] reported that the range of multifractality (nonuniformity of the measure) exhibited a sharp peak when the type of serrations transitioned from type B to A. This transition was associated with a change from the chaotic to self-organized criticality behavior [63].

More recently, Kantelhardt *et al.* developed the MFDFA technique to estimate the multifractal spectrum of different stochastic processes [51,64]. This method has been used to analyze different phenomena, including financial time series [64,65], hydrological data [66], seismic activity [67,68], and electroencephalography signals [69,70]. Note that the MFDFA algorithm can require a definite scaling range to estimate the related scaling exponents, which is sometimes difficult to determine [71]. The details of the application of the MFDFA technique are given in the Supplemental Material [49] and Refs. [35,51,68,72].

By applying MFDFA to our time-series data, the factors that characterize the scaling behavior of DPF were determined. These factors include the local singularity strength, α, and the fractal dimension, $f(\alpha)$, of the subset of intervals that are characterized by the singularity strength [61]. From the results, plots of $f(\alpha)$ vs α, known as the multifractal spectrum, are obtained. An important quantity is the width of the multifractal spectrum, which describes the multifractality of the dataset and is generally denoted as $\Delta = \alpha_{max} - \alpha_{min}$. The multifractality is characterized by a scale invariance of multiple exponents and multiscale correlations in the underlying physical process [56]. In the present context, an increase in Δ is associated with an increase in the irregularity of the DPF behavior [56].

Figure 4 displays the multifractal spectral results for the samples tested at 0.5, 2.1, and 4.2 K, as determined by the MFDFA technique. It was found that the maximum value of f was ∼1, which suggests that the events responsible for the multifractal character are roughly uniformly distributed in time [52]. In addition, the wide spectra are a footprint of long-range time correlations involving an extended set of scaling indices [73]. With an increase in the temperature, there was a shift of the spectra to greater α values. Furthermore, the multifractality of the data was found to increase [see Fig. 4(b)], suggesting that the heterogeneity of the DPF increased with an increase in the test temperature. Figure 4(c) shows a plot of the A_{se} vs Δ data. One can see a strong linear correlation between the complexity and the
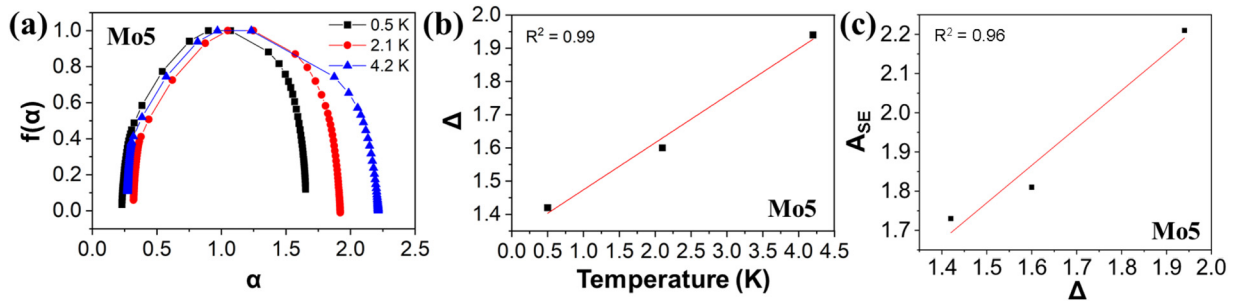
FIG. 4. MFDFA results showing (a) the multifractal spectrum; (b) $\Delta = \alpha_{max} - \alpha_{min}$ for samples tested at 0.5, 2.1, and 4.2 K; and (c) the A_{SE} vs Δ plot for the samples tested at the three temperatures.

multifractality of the DPF. The relatively large R^2 value of 0.99 indicates that there was a high degree of positive correlation between the multifractality of the DPF and the temperature. Furthermore, the results also indicate that at deep cryogenic temperatures, the increasing inhomogeneity of the stress-drop behavior is strongly related (R^2 value of 0.96) to the degree of complexity of the serration dynamics during plastic deformation.

VI. DISCUSSION

In the previous work [24], the DPF of the Mo5 alloy was associated with the dislocation locking and avalanche-type breakaway from the barriers, such as μ-phase precipitates and deformation-induced body-centered-cubic (bcc) martensite. The thermal activation of cross slip is inhibited during the deformation at deep cryogenic temperatures (0.5–4.2 K) [24]. As a result, severe strain localization occurs in shear bands, as observed in Fig. 1(d). The μ precipitates and bcc martensite substantially enhance the yield strength and the strain hardening rate of the alloy through precipitation hardening and DIMT. They also affect DPF by serving as sites for strain localization at temperatures below 4.2 K. This is a major DPF-related difference between the present Mo5 alloy and the fcc single-phase MPEAs [17,18]. In the latter, the barriers obstructing dislocation motion were associated with the Lomer–Cottrell locks [17,18]. Additional barriers formed during deformation of single-phase MPEAs, including deformation-induced twins and hexagonal close-packed (hcp) martensite particles, are not considered to affect DPF [18]. By contrast, the bcc martensite formed in the Mo5 alloy may influence DPF significantly. During stress drops under DPF, the release of the strain energy generates heat under near-adiabatic conditions, and the local temperature is raised [24]. As the test temperature decreases down to 0.5 K, the adiabatic heating becomes more pronounced because both the thermal conductivity and the heat capacity approach zero [9,24]. At the same time, the dislocation density during plastic deformation in the temperature range of 0.5–4.2 K is reduced with decreasing test temperature as dynamic recovery is promoted by adiabatic heating [24].

An almost periodic recurrence of the large avalanches over 100 MPa (see Fig. 2) strongly suggests that a strain-softening mechanism is at play. If dislocation glide occurs at a "weak spot", it becomes easier for following dislocations to glide

at the same location [35–38]. This feature is consistent with the observed occurrence of localized shear bands [Fig. 1(d)] in the temperature interval considered, which also reflects deformation softening.

As shown in Figs. 3 and 4, the complexity and heterogeneity of the DPF were attenuated below 4.2 K. This increase in the complexity and heterogeneity may be associated with a greater dislocation density in samples deformed at higher temperatures within the temperature range considered (0.5–4.2 K) [24]. In this scenario, a larger number of dislocations are available to participate in the dislocation pinning and pileup formation processes at higher temperatures. Consequently, a greater variety of interactions gives rise to a more complex behavior during the avalanche slip [42,43]. The increase in complexity (see Figs. 3 and 4) also suggests a greater degree of spatial correlations between the avalanche events. This feature means that dislocation avalanches are less localized in space and time and do not exhibit a definite characteristic magnitude [56]. Furthermore, the increase in complexity leads to a more heterogeneous discontinuous plastic flow, as indicated by the results of the multifractal analysis (see Fig. 4). Enhanced heterogeneity is a consequence of a higher density of dislocations that lead to increased dislocation locking and strain hardening. This trend impedes the propagation of deformation bands and the relaxation of strain gradients they produce [62]. It should be noted that an erratic behavior of DPF can be attributed to the heterogeneity of deformation irrespective of the specific material considered [42,61,74].

Lastly, it is important to mention the relationship between the temperature-dependent complexity and multifractal results, which is evident in Fig. 4(c). This result demonstrates that there exists a strong correlation between the multifractality and the complexity of the discontinuous plastic flow. In other words, an increase in the complexity of the dynamics of DPF corresponds to a greater degree of multiscale correlations in the underlying physical process [56].

VII. CONCLUSIONS

In this paper, we have investigated the periodicity and heterogeneity of the discontinuous plastic flow of the Mo5 alloy at the liquid helium temperature and below—down to the low temperature of 0.5 K. To that end, state-of-the-art statistical data analysis techniques were employed. The nearly periodic occurrence of large slip avalanches associated with stress

drops implies that a strain-softening mechanism is involved. It manifests itself in strain localization in shear bands. Within the temperature range of 0.5–4.2 K, the heterogeneity and complexity of processes underlying the serrated appearance of the deformation curves are reduced when the test temperature is decreased. We provided an explanation for this unexpected temperature dependence of the complexity of the discontinuous plastic flow of the Mo5 alloy. It was accounted for by a reduction of the dislocation density due to the local temperature rise associated with adiabatic heating that accompanies stress drops, the effect becoming greater as the deformation temperature is lowered. Besides, it may be important to extend the analytical techniques used in the current work to other types of dynamical behavior associated with the serrated flow, such as acoustic emission measurements. The critical temperature at which the discontinuous plastic flow sets in lies above 4.2 K, but its exact magnitude is yet to be determined.

The link between the irregularity and the scaling behavior of the discontinuous plastic flow at deep cryogenic temperatures established in this paper calls for further study. Future work should focus on identifying the physical mechanisms underlying discontinuous plastic flow based on the features of the stress-drop statistics uncovered in the present work. To that end, shear localization during cryogenic deformation will be investigated by *in situ* acoustic emission, which can discriminate between the individual deformation mechanisms.

[1] Y.-M. Yang, J.-H. Kim, H.-S. Seo, K. Lee, and I.-S. Yoon, in *Proceedings of the 23rd World Gas Conference* (International Gas Union, Amsterdam, 2006), pp. 1–14.

[2] J. Kolowrotkiewicz, M. Barański, W. Szeleg, and L. Długiewicz, COMPEL-Int. J. Comput. Math. Electr. Electron. Eng. **26**, 952 (2007).

[3] https://wmap.gsfc.nasa.gov/universe/bb_cosmo_fluct.html.

[4] N. V. Isaev, V. D. Natsik, V. V. Pustovalov, V. S. Fomenko, and S. É. Shumilin, Low. Temp. Phys. **31**, 898 (2005).

[5] A. I. Landau, Phys. Stat. Sol. A **65**, 415 (1981).

[6] V. V. Pustovalov, Fiz. Nizk. Temp. **26**, 515 (2000) [Sov. J. Low Temp. Phys. **26**, 375 (2000)].

[7] Y. Zhang, J. P. Liu, S. Y. Chen, X. Xie, P. K. Liaw, K. A. Dahmen, J. W. Qiao, and Y. L. Wang, Prog. Mater. Sci. **90**, 358 (2017).

[8] Z. G. Cheng and J. Beamish, Phys. Rev. Lett. **121**, 055301 (2018).

[9] B. Skoczen, J. Bielski, S. Sgobba, and D. Marcinek, Int. J. Plast. **26**, 1659 (2010).

[10] B. Obst and A. Nyilas, Mater. Sci. Eng. A **137**, 141 (1991).

[11] M. A. Laktionova, E. D. Tabachnikova, Z. Tang, and P. K. Liaw, Fiz. Nizk. Temp. **39**, 814 (2013) [Sov. J. Low Temp. Phys. **39**, 630 (2013)].

[12] Y. Estrin and L. P. Kubin, Scr. Metall. **14**, 1359 (1980).

[13] X. Guo, X. Xie, J. Ren, M. Laktionova, E. Tabachnikova, L. Yu, W.-S. Cheung, K. A. Dahmen, and P. K. Liaw, Appl. Phys. Lett. **111**, 251905 (2017).

[14] M. Koslowski, R. LeSar, and R. Thomson, Phys. Rev. Lett. **93**, 125502 (2004).

[15] J. Tabin, B. Skoczen, and J. Bielski, Int. J. Solids Struct. **97-98**, 593 (2016).

[16] A. Seeger, Philos. Mag. **46**, 1194 (1955).

[17] M. Naeem, H. He, F. Zhang, H. Huang, S. Harjo, T. Kawasaki, B. Wang, S. Lan, Z. Wu, F. Wang, Y. Wu, Z. Lu, Z. Zhang, C. T. Liu, and X.-L. Wang, Sci. Adv. **6**, eaax4002 (2020).

[18] A. S. Tirunilai, T. Hanemann, K.-P. Weiss, J. Freudenberger, M. Heilmaier, and A. Kauffmann, Acta Mater. **200**, 980 (2020).

[19] J. Liu, X. Guo, Q. Lin, Z. He, X. An, L. Li, P. K. Liaw, X. Liao, L. Yu, J. Lin, L. Xie, J. Ren, and Y. Zhang, Sci. China Mater. **62**, 853 (2019).

[20] S. Xia and Y. Zhang, Mater. Sci. Eng. A **733**, 408 (2018).

[21] J. Antonaglia, X. Xie, Z. Tang, C. W. Tsai, J. W. Qiao, Y. Zhang, M. O. Laktionova, E. D. Tabachnikova, J. W. Yeh, O. N. Senkov, M. C. Gao, J. T. Uhl, P. K. Liaw, and K. A. Dahmen, JOM **66**, 2002 (2014).

[22] E. D. Tabachnikova, A. V. Podolskiy, M. O. Laktionova, N. A. Bereznaia, M. A. Tikhonovsky, and A. S. Tortika, J. Alloys Compd. **698**, 501 (2017).

[23] J. Brechtl, S. Chen, C. Lee, Y. Shi, R. Feng, X. Xie, D. Hamblin, A. M. Coleman, B. Straka, H. Shortt, R. J. Spurling, and P. K. Liaw, Metals **10**, 1101 (2020).

[24] J. Moon, E. Tabachnikova, S. Shumilin, T. Hryhorova, Y. Estrin, J. Brechtl, P. K. Liaw, W. Wang, K. A. Dahmen, A. Zargaran, J. W. Bae, and H. S. Kim, Mater. Today (to be published).

[25] L. Proville, D. Rodney, and M. C. Marinica, Nat. Mater. **11**, 845 (2012).

[26] B. V. Petukhov, Fiz. Nizk. Temp. **12**, 749 (1986) [Sov. J. Low Temp. Phys. **12**, 425 (1986)].

[27] I. N. Kuzmenko and V. V. Pustovalov, Cryogenics **25**, 346 (1985).

[28] J. Hirsch and K. Lücke, Acta Metall. **36**, 2863 (1988).

[29] H. Bi, G. Börner, and Y. Chu, Astron. Astrophys. **218**, 19 (1989).

[30] L. W. McFaul, W. J. Wright, X. Gu, J. T. Uhl, and K. A. Dahmen, Phys. Rev. E **97**, 063005 (2018).

[31] J. Baró, J.-M. Martín-Olalla, F. J. Romero, M. C. Gallardo, E. K. H. Salje, E. Vives, and A. Planes, J. Phys.: Condens. Matter **26**, 125401 (2014).

[32] K. A. Dahmen, Y. Ben-Zion, and J. T. Uhl, Phys. Rev. Lett. **102**, 175501 (2009).

[33] R. Carroll, C. Lee, C.-W. Tsai, J.-W. Yeh, J. Antonaglia, B. Brinkman, M. LeBlanc, X. Xie, S. Chen, P. K. Liaw, and K. A. Dahmen, Sci. Rep. **5**, 16997 (2015).

[34] J. Antonaglia, W. J. Wright, X. Gu, R. R. Byer, T. C. Hufnagel, M. LeBlanc, J. T. Uhl, and K. A. Dahmen, Phys. Rev. Lett. **112**, 155501 (2014).

[35] M. A. Lebyodkin, Y. Bréchet, Y. Estrin, and L. P. Kubin, Phys. Rev. Lett. **74**, 4758 (1995).

[36] Y. Estrin and Y. Bréchet, Pure Appl. Geophys. **147**, 745 (1996).

[37] M. A. Lebyodkin, Y. Bréchet, Y. Estrin, and L. P. Kubin, Solid State Phenom. **42-43**, 313 (1995).

[38] W. McFaul, Ph.D. thesis, University of Illinois at Urbana-Champaign, 2018.

[39] J. Brechtl, X. Xie, P. K. Liaw, and S. J. Zinkle, Chaos Soliton. Fract. **116**, 166 (2018).

[40] E. Blons, L. M. Arsac, P. Gilfriche, and V. Deschodt-Arsac, Entropy **21**, 1024 (2019).

[41] J. Escudero, E. Acar, A. Fernandez, and R. Bro, Brain Res. Bull. **119**, 136 (2015).

[42] J. Brechtl, B. Chen, X. Xie, Y. Ren, J. D. Venable, P. K. Liaw, and S. J. Zinkle, Mater. Sci. Eng. A **753**, 135 (2019).

[43] A. Sarkar, A. Chatterjee, P. Barat, and P. Mukherjee, Mater. Sci. Eng. A **459**, 361 (2007).

[44] B. Zhang, P. K. Liaw, J. Brechtl, J. Ren, X. Guo, and Y. Zhang, J. Alloys Compd. **820**, 153092 (2020).

[45] M. Costa, A. L. Goldberger, and C. K. Peng, Phys. Rev. E **71**, 021906 (2005).

[46] M. D. Costa and A. L. Goldberger, Entropy **17**, 1197 (2015).

[47] S.-D. Wu, C.-W. Wu, S.-G. Lin, K.-Y. Lee, and C.-K. Peng, Phys. Lett. A **378**, 1369 (2014).

[48] A. Humeau-Heurtier, Entropy **17**, 3110 (2015).

[49] See Supplemental Material at http://link.aps.org/supplemental/10.1103/PhysRevMaterials.5.083601 for details of RCMSE analysis and MFDFA method.

[50] E. A. F. Ihlen, Front. Physiol. **3**, 141 (2012).

[51] J. W. Kantelhardt, S. A. Zschiegner, E. Koscielny-Bunde, S. Havlin, A. Bunde, and H. E. Stanley, Physica A **316**, 87 (2002).

[52] M. A. Lebyodkin and T. A. Lebedkina, Phys. Rev. E **77**, 026111 (2008).

[53] M. S. Bharathi, M. Lebyodkin, G. Ananthakrishna, C. Fressengeas, and L. P. Kubin, Phys. Rev. Lett. **87**, 165508 (2001).

[54] T. A. Lebedkina and M. A. Lebyodkin, Acta Mater. **56**, 5567 (2008).

[55] T. A. Lebedkina, M. A. Lebyodkin, T. T. Lamark, M. Janeček, and Y. Estrin, Mater. Sci. Eng. A **615**, 7 (2014).

[56] M. A. Lebyodkin, N. P. Kobelev, Y. Bougherira, D. Entemeyer, C. Fressengeas, T. A. Lebedkina, and I. V. Shashkov, Acta Mater. **60**, 844 (2012).

[57] M. A. Lebyodkin, T. A. Lebedkina, and A. Jacques, *Multifractal Analysis of Unstable Plastic Flow* (Nova Science Publishers, Inc., New York, 2009).

[58] M. A. Lebyodkin and T. A. Lebedkina, Phys. Rev. E **73**, 036114 (2006).

[59] J. L. Ren, C. Chen, Z. Y. Liu, R. Li, and G. Wang, Phys. Rev. B **86**, 134303 (2012).

[60] E. C. Aifantis, in *Advances in Applied Mechanics*, edited by S. P. A. Bordas and D. S. Balint (Elsevier, Amsterdam, 2012), Vol. 49, pp. 1–110.

[61] J. Brechtl, S. Y. Chen, X. Xie, Y. Ren, J. W. Qiao, P. K. Liaw, and S. J. Zinkle, Int. J. Plast. **115**, 71 (2019).

[62] M. A. Lebyodkin and Y. Estrin, Acta Mater. **53**, 3403 (2005).

[63] Z. Olami, H. J. S. Feder, and K. Christensen, Phys. Rev. Lett. **68**, 1244 (1992).

[64] J. R. Thompson and J. R. Wilson, Math. Comput. Simul. **126**, 63 (2016).

[65] L. Yang, Y. Zhu, and Y. Wang, Physica A **451**, 357 (2016).

[66] X. Zhang, G. Zhang, L. Qiu, B. Zhang, Y. Sun, Z. Gui, and Q. Zhang, Water **11**, 891 (2019).

[67] X. Fan and M. Lin, Physica A **479**, 225 (2017).

[68] L. Telesca and L. Toth, Physica A **448**, 21 (2016).

[69] A. K. Maity, R. Pratihar, A. Mitra, S. Dey, V. Agrawal, S. Sanyal, A. Banerjee, R. Sengupta, and D. Ghosh, Chaos Soliton. Fract. **81**, 52 (2015).

[70] T. Zorick and M. A. Mandelkern, PLoS One **8**, e68360 (2013).

[71] D. Nian and Z. T. Fu, Commun. Nonlinear Sci. Numer. Simul. **67**, 568 (2019).

[72] D. Gulich and L. Zunino, Physica A **391**, 4100 (2012).

[73] J. Weiss, T. Richeton, F. Louchet, F. Chmelik, P. Dobron, D. Entemeyer, M. Lebyodkin, T. Lebedkina, C. Fressengeas, and R. J. McDonald, Phys. Rev. B **76**, 224110 (2007).

[74] J. Brechtl, X. Xie, Z. Wang, J. Qiao, and P. K. Liaw, Mater. Sci. Eng. A **771**, 138585 (2020).